

## DESIGN OF BROADBAND AND POLARIZATION-INDEPENDENCE METAMATERIAL ABSORBER USING A CHIRAL STRUCTURE WITH CONDUCTIVE POLYMER

Tong Ba Tuan<sup>1</sup>, Bui Huu Nguyen<sup>1</sup>, Nguyen Thi Hau<sup>1</sup>, Tran Van Huynh<sup>2</sup>,  
Vu Dinh Lam<sup>2</sup> and Le Dac Tuyen<sup>1,\*</sup>

<sup>1</sup>*Department of Physics, Hanoi University of Mining and Geology*

<sup>2</sup>*Graduate University of Science and Technology,  
Vietnam Academy of Science and Technology*

**Abstract.** We present a simple approach to enhance the bandwidth and absorptivity of the metamaterial absorber (MA) in the GHz region. The proposed MA is designed and simulated by computer simulation technology (CST) Microwave Studio. The results indicate that the absorption of the MA strongly depends on the conductivity of the polymer. By using a chiral structure with the low conductive polymer of 700 S/m, the absorption bandwidth is expanded up to 12.9 GHz (relative bandwidth of 85.7%) with absorptivity over 80%. It exhibits polarization-independent absorption and can be applied to fabricate broadband MA.

**Keywords:** metamaterials, metamaterial absorber, chiral structure, conductive polymer.

### 1. Introduction

Metamaterial is an artificial structure designed to achieve the desired properties that natural materials do not exhibit [1]. In recent years, great efforts have been made to change their permittivity and permeability to create unique materials in negative refractive index or control electromagnetic wave [1-3]. Since the pioneering work of Landy *et al.* [4], metamaterial absorber (MA) has attracted a lot of attention because of its ultrathin thickness and tailoring frequency compared to traditional absorbers [4, 5]. MA has been demonstrated in applications, such as solar energy harvesting, biological sensing, imaging device, and photodetection [4-9].

MA is often formed by the periodic arrangement of unit cells which consists of a subwavelength resonator structure and a ground plane separated by a dielectric layer [4, 5]. However, MA often provides a narrow absorption bandwidth, which may limit its applications. By adjusting the structure and geometric parameters of the unit cell, single-

---

Received May 5, 2021. Revised June 13, 2021. Accepted June 20, 2021.

Contact Le Dac Tuyen, e-mail address: [ledactuyen@humg.edu.vn](mailto:ledactuyen@humg.edu.vn)

or multiple-band absorption can be achieved at resonant frequencies. A great effort has been made to expand the absorption bandwidth [5, 10-15]. One approach is to utilize multi-resonance by incorporating multi-sized or multi-shaped resonators within one unit [10], and multiple metal-dielectric layers [11]. Recently, Tran *et al.* presented a broadband GHz absorber based on controlled defects [12]. The number and position of the defects in a full-size structure were optimized with different configurations. Tiep *et al.* demonstrated a wideband absorber using hybrid materials [13]. The thickness of MA is only 0.4 mm ( $\lambda/82$ ) at the working frequency in the GHz region. Pham *et al.* reported a near-field effect to create dual-band MA [14]. The electromagnetic (EM) wave in the infrared regime is also absorbed by the multi-configuration of nanocluster [15]. However, the designs are mostly based on symmetrical resonator structures. The asymmetric or chiral structures have often been studied to make negative refractive materials due to their ability to interact with EM waves [16]. The chiral structure, which does not overlap with mirror symmetry image, can be proposed as an alternative resonator for MA with high absorptivity [17]. The chiral structures exhibit different properties upon interactions with circularly polarized light of opposite handedness. For each chiral structure design, there exists an inverted design that reverses the optical response perfectly. New structures, as well as studying new properties to improve operational efficiency, is always a challenge for research groups.

In this work, we demonstrate an effective model to enhance the bandwidth and absorptivity of MA by using a chiral structure and conductive polymer. The structure was proposed and simulated by using a commercial computer simulation technology (CST) Microwave Studio. The broadband MA is achieved by optimizing the conductivity of the polymer. The absorption mechanism is discussed and analyzed via surface current and electromagnetic field distributions. Moreover, the proposed design exhibit polarization-independent absorption with a wide range of incident angles.

## **2. Content**

### **2.1. Structure and design**

Figure 1 illustrates the schematic diagram and geometric parameters of the proposed MA. The unit-cell of the MA consists chiral resonator structure that is embedded in the front of the FR-4 dielectric substrate, and the copper layer covers the whole backside. The geometric parameters of MA are periodicity of  $p = 6$  mm, chiral structure diameters of  $a = 4$  mm,  $b = 2$  mm,  $c = 0.7$  mm,  $t_p = 0.15$  mm. The FR-4 substrate has a dielectric constant of 4.4, a loss tangent of 0.025, and thickness  $t_d = 2$  mm. The copper layer has an electrical conductivity  $\sigma = 5,8 \times 10^7$  S/m and thickness  $t_m = 0.036$  mm. For studying the absorption behaviors, the electrical conductivity of polymer is adjusted, and the width of chiral structure  $c$  is varied. The chiral structure becomes square (symmetric structure) when the width  $c = 4/3$  mm.

The proposed MA was designed and simulated by commercial CST Microwave Studio. The EM wave with polarization angle ( $\varphi$ ) and incident angle ( $\theta$ ) is shown in Figure 1, where the periodic structure is illuminated by an incident plane wave with the electric field parallel to the x-axis (TE mode). Perfectly matched layers are applied along

the z-direction and periodic boundary conditions in the x and y-directions. The absorption of a MA is defined as  $A = 1 - R - T = 1 - |S_{11}|^2 - |S_{12}|^2$ , where the  $S_{11}$  and  $S_{12}$  are reflection and transmission coefficients. Due to the continuous copper covering on the bottom layer of MA, the transmission is blocked  $T = |S_{12}|^2 = 0$ , the absorption is simple calculated by  $A = 1 - |S_{11}|^2$ , where  $|S_{11}|^2 = R$  is reflection [13, 18].

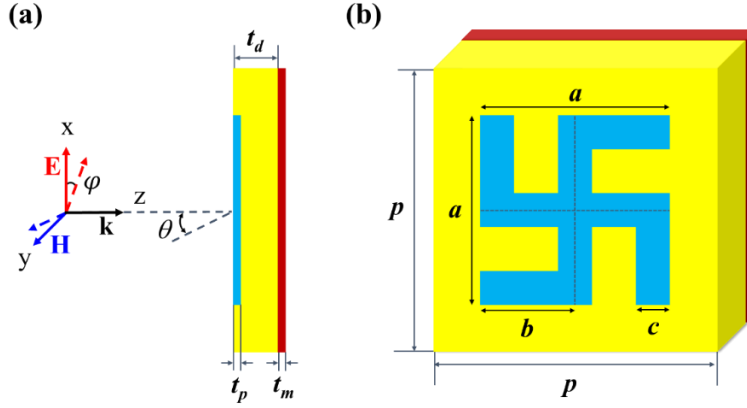


**Figure 1. A schematic diagram of the unit cell of MA with structural parameters and incident electromagnetic wave: (a) side view and (b) 3D view.  $p = 6$  mm,  $a = 4$  mm,  $b = 2$  mm,  $c = 0.7$  mm,  $t_d = 2$  mm,  $t_p = 0.15$  mm, and  $t_m = 0.036$  mm**

## 2.2. Result and discussion

Figure 2(a) shows a comparison of the absorption spectra between copper MA and polymer MA with different conductivity in the frequency range of 5 - 25 GHz. For copper MA ( $\sigma = 5.8 \times 10^7$  S/m), the absorption spectra have two resonant peaks at around 9.6 GHz ( $f_1$ ) and 21.1 GHz ( $f_2$ ) with the absorptivity of 30% and 40%, respectively. When the conductivity of polymer decreases, the absorption peaks are slightly shifted and the absorptivity increases. However, the absorptivity of the polymer MA is not proportional to conductivity with the same simulation setup condition. When the conductivity of polymer is 700 S/m, two absorption peaks are 10 GHz and 18.8 GHz with absorptivity up to 96% ( $f_1$ ) and 99% ( $f_2$ ). This yields wideband absorption over 80% from 8.6 to 21.5 GHz (relative bandwidth of 85.7%). Two absorption peaks overlap into one peak when the conductivity of polymer decreases to 300 S/m. This manifestly reveals that the conductivity of the polymer plays an important role to obtain higher absorptivity of the designed MA.

To understand the absorption mechanism of the MA, we have simulated the surface current and electric field distributions at two resonant frequencies of 9.7 and 21.1 GHz as shown in Figure 3. For the lower resonant frequency  $f_1 = 9.7$  GHz, the surface currents on the front and back layers are antiparallel, and the electric field is mainly focused on the top and bottom following the electric direction of the EM wave. Meanwhile, for the higher resonant frequency  $f_2 = 21.1$  GHz, the surface currents on the front and back layers are parallel, and the electric field is concentrated at part of the MA. It indicates that the lower frequency is attributed to magnetic resonance [10]. While the higher frequency

is the electric resonance [19]. The absorption properties of the designed MA are due to the strong resonance that can be excited by both electric and magnetic fields.

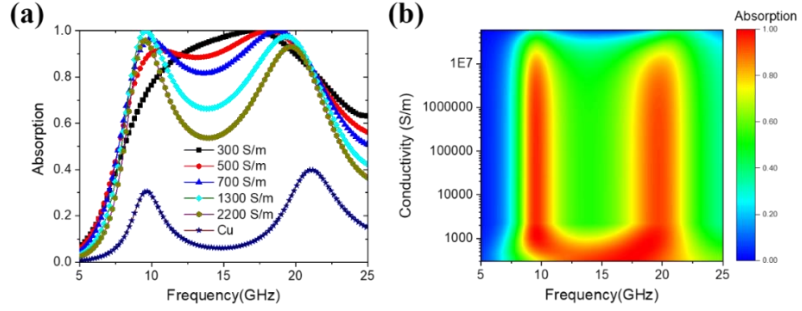


**Figure 2. (a) Absorption spectra and (b) absorption map of the chiral structure MA with various conductivity of the polymer, (b)  $p = 6$  mm,  $a = 4$  mm,  $b = 2$  mm,  $c = 0.7$  mm,  $t_d = 2$  mm,  $t_p = 0.15$  mm, and  $t_m = 0.036$  mm**

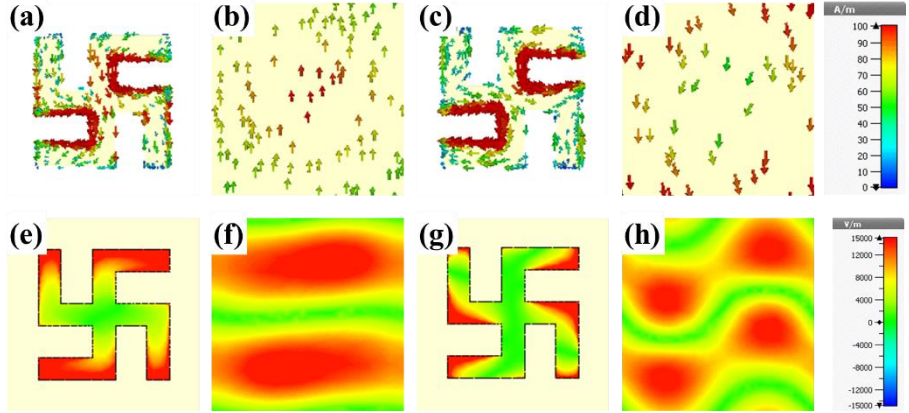


**Figure 3. Distributions of surface currents on (a, c) the front and (b, d) back layers corresponding to electric field distribution on (e, f) the front and (g, h) back layers of the MA at (a, b, e, f) 9.7 GHz and (c, d, g, h) 21.1 GHz, respectively**

In addition, the absorption behavior of the copper and polymer MA can be explained by impedance matching which is calculated via  $S$ -parameters as [12, 20]

$$Z = \sqrt{\frac{(1 + S_{11})^2 - S_{21}^2}{(1 - S_{11})^2 - S_{21}^2}} = \frac{1 + S_{11}}{1 - S_{11}}.$$

At certain frequencies the effective impedance, which is defined as  $Z(\omega) = \sqrt{\mu(\omega)/\epsilon(\omega)}$ , matches to the free space impedance ( $\text{Re}(Z) = 1$ ,  $\text{Im}(Z) = 0$ ), and therefore the reflection is minimized  $|S_{11}|^2 = 0$ . The real and imaginary parts of the effective impedance for the copper and polymer MAs are presented in Figures 4(a) and 4(b), respectively. For the copper MA, the effective impedance is not matched with free space at resonant frequencies of 9.7 and 21.1 GHz. Meanwhile, for the polymer MA, the real and imaginary parts of the effective impedance are approximately 1 and 0 at both resonant

frequencies of 10 GHz and 18.8 GHz, respectively. Furthermore, the effective impedance of polymer MA not only matches with that of free space better than copper but also in a wide frequency range from 9 to 21 GHz. It is reasonable to explain that the absorptivity of the polymer MA is higher than the copper MA. Low conductivity polymer has improved the impedance matching to enhance absorptivity.

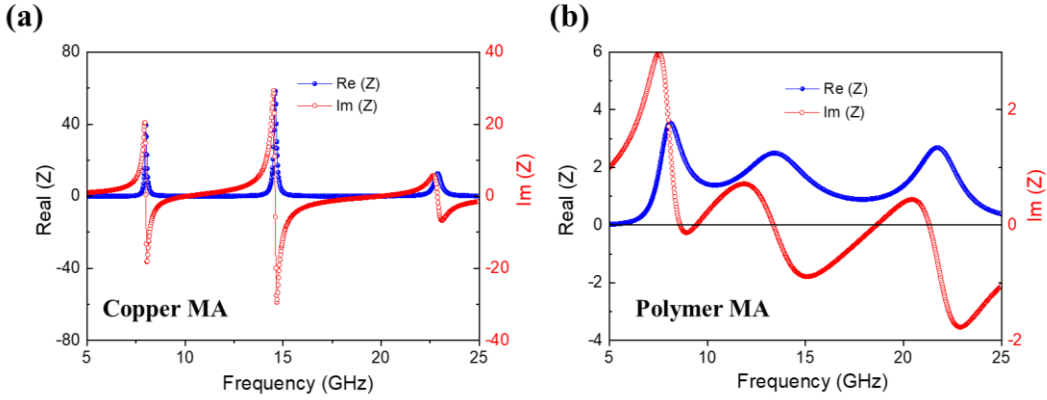


**Figure 4.** The effective impedance of (a) copper MA  $\sigma = 5.8 \times 10^7$  S/m and (b) polymer MA  $\sigma = 700$  S/m

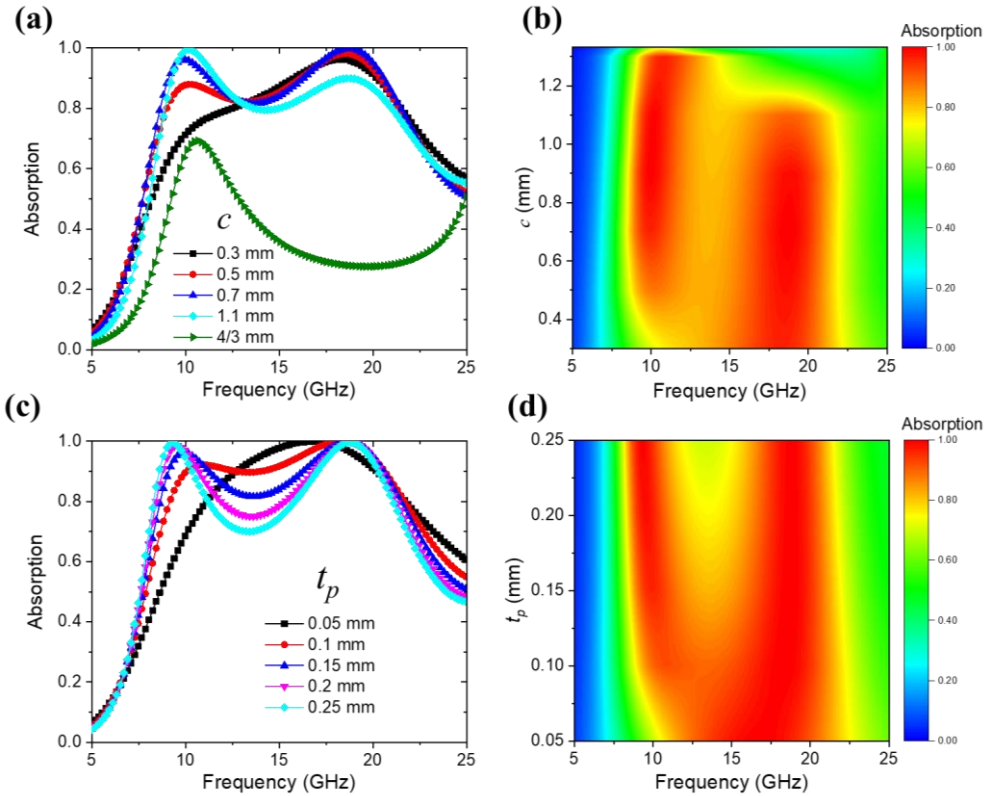


**Figure 5.** Dependence of absorption spectra on (a), (b) width  $c$  and (c), (d) thickness  $t_p$  of polymer chiral structure

To evaluate the influence of structure parameters on absorption behavior, the width  $c$  and thickness  $t_p$  of the chiral structure are varied. Figures 5(a) and 5(b) show the dependence of absorption spectra on varying  $c$  from 0.3 to 4/3 mm. When the width  $c$  has the value of 0.3 - 1.1 mm, the absorption spectra exhibit two peaks with little change of absorptivity. However, for  $c = 4/3$  mm, the chiral structure becomes a square shape, and the absorption spectrum exhibits only one peak that coincides with the low resonant frequency  $f_1$ . As we know that the square structure is a symmetry resonator, which often drives magnetic resonances [19, 21]. It indicates that the chiral structure can create two absorption peaks to gain wider bandwidth of MA. The dependence of absorption spectra of polymer MA on thickness  $t_p$  is presented in Figures 5(c) and 5(d). When the thickness decreases from 0.25 to 0.05 mm, the two absorption peaks are shifted to opposite directions and merge into one absorption peak. The calculated skin depth is about 0.5 mm, which is much greater than the proposed thickness  $t_p$  of chiral structure with low conductivity. So, the low conductivity of the polymer plays an important role to enhance absorptivity and broadband absorption.

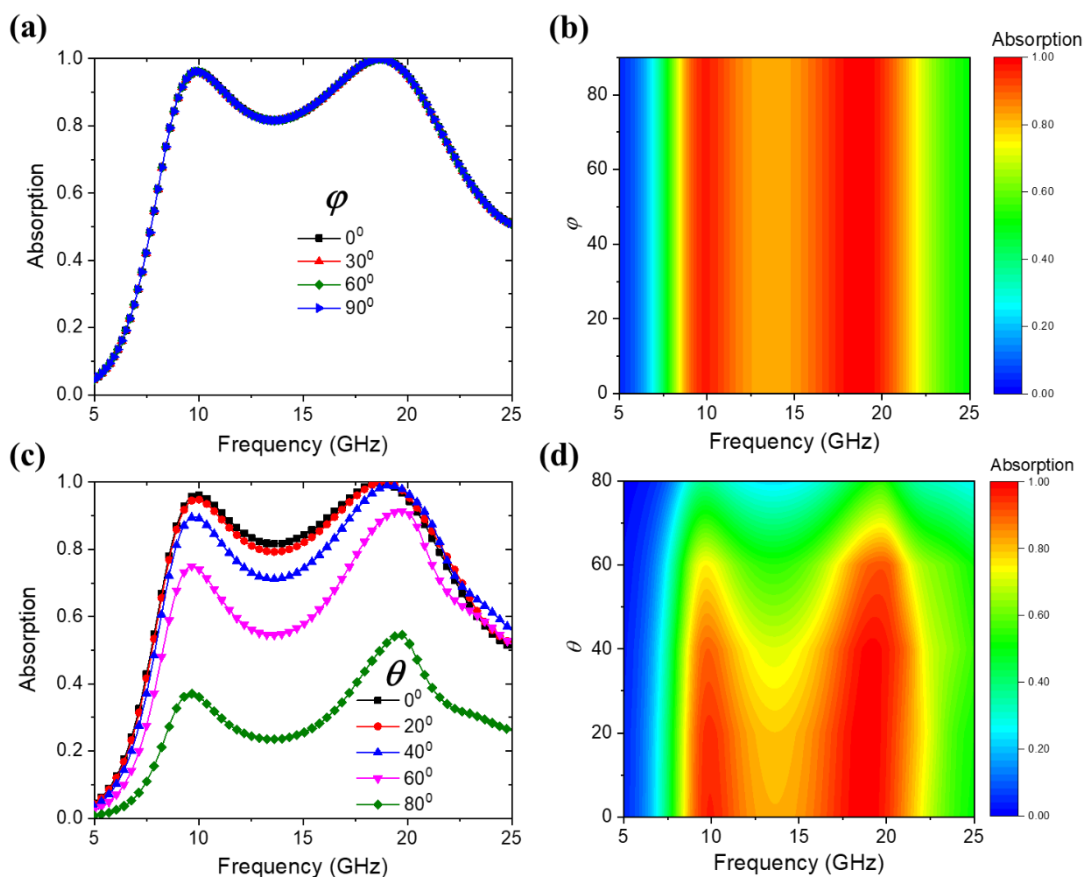


**Figure 6.** Dependence of absorption spectra on (a, b) the polarization angle  $\phi$  and (c, d) incident angle  $\theta$

Figures 6(a) and 6(b) present the absorption spectra according to the different polarization angle  $\varphi$  with normal EM wave. By rotating the emitting/receiving horn antenna or the MA structure, the absorption lines consist in the range of polarization angle  $\varphi$  from  $0^\circ$  to  $90^\circ$ . It is attributed to metasurface properties of chiral structure [17, 22]. The observed results suggest that the incident and reflected EM waves from the copper plane are rotated in the opposite direction when it goes through chiral structure, resulting in polarization-independence of absorption spectra. The influence of oblique incident angle on absorption spectra of polymer MA is presented in Figures 6(c) and 6(d). The results exhibit that the absorptivity is slightly changed in the range from  $0^\circ$  to  $40^\circ$  of incidence angle. When the incident angle is larger than  $60^\circ$ , the absorptivity is rapidly decreased. This is attributed to the geometry of the chiral structure, in which the absorption properties are nearly isotropic at a small incident angle and manifested at a large incident angle.

### 3. Conclusions

The numerical investigation of MA using the chiral structure and conductive polymer is studied. The absorption properties of the proposed MA depend on the electrical conductivity of the polymer. When the conductivity of polymer is 700 S/m, the absorption bandwidth is up to 12.9 GHz with absorptivity over 80%. The MA is also independent of polarization and large incident angle. The design can be applied to fabricate broadband MA and for higher frequency regimes.

**Acknowledgment.** This work is supported by Hanoi University of Mining and Geology (grant number T20-02) and the Ministry of Education and Training, Vietnam (grant number B2020-MDA-10).

### REFERENCES

- [1] D. Smith, W. J. Padilla, D. Vier, *et al.*, 2000. Composite medium with simultaneously negative permeability and permittivity. *Phys. Rev. Lett.*, **84**, 4184.
- [2] P. Ball, 2018. Bending the laws of optics with metamaterials: an interview with John Pendry. *National Science Review*, **5**, 200-202.
- [3] J. B. Pendry, D. Schurig, D. R. Smith, 2006. Controlling Electromagnetic Fields. *Science*, **312**, 1780.
- [4] N. Landy, S. Sajuyigbe, J. Mock, D. Smith, W. Padilla, 2008. Perfect metamaterial absorber. *Phys. Rev. Lett.*, **100**, 207402.
- [5] P. Yu, L. V. Besteiro, Y. Huang *et al.*, 2019. Broadband Metamaterial Absorbers. *Adv. Optical Mater.*, **7**, 1800995.
- [6] L. Luo, I. Chatzakis, J. Wang, *et al.*, 2014. Broadband terahertz generation from metamaterials. *Nat. Commun.*, **5**, 3055.
- [7] T. S. Bui, T. D. Dao, L. H. Dang, *et al.*, 2016. Metamaterial-enhanced vibrational absorption spectroscopy for the detection of protein molecules. *Sci. Rep.*, **6**, 32123.

- [8] B.D.F. Casse, W.T. Lu, Y.J. Huang, *et al.*, 2010. Super-resolution imaging using three-dimensional metamaterials nanolens. *Appl. Phys. Lett.*, **96**, 023114.
- [9] K.T. Lin, H.L. Chen, Y.S. Lai, *et al.*, 2014. Silicon-based broadband antenna for high responsivity and polarization-insensitive photodetection at telecommunication wavelengths. *Nat. Commun.*, **5**, 3288.
- [10] D. T. Viet, N. T. Hien, P. V. Tuong, *et al.*, 2014. Perfect absorber metamaterials: peak, multi-peak, and broadband absorption. *Opt. Commun.*, **322**, 209-213.
- [11] Y. J. Kim, Y. J. Yoo, K. W. Kim, *et al.*, 2015. Dual broadband metamaterial absorber. *Opt. Express*, **23**, 3861.
- [12] M. C. Tran, D. H. Le, V. H. Pham, *et al.*, 2018. Controlled Defect Based Ultra-Broadband Full-sized Metamaterial Absorber. *Sci. Rep.*, **8**, 9523.
- [13] D. H. Tiep, B. X. Khuyen, B. S. Tung, *et al.*, 2018. Enhanced-bandwidth perfect absorption based on a hybrid metamaterial. *Opt. Mater. Express*, **8**, 2751-2759.
- [14] T. L. Pham, H. T. Dinh, D. H. Le, *et al.*, 2020. Dual-band Isotropic Metamaterial Absorber Based on Near-field Interaction in The Ku Band. *Curr. Appl. Phys.*, **20**, 331-336.
- [15] T.M. Cuong, K.H. Trang, D.H. Tung, *et al.*, 2019. Electromagnetic properties of multi-configuration of gold nano cluster absorber in infrared regime. *HNUE J. Sci.*, **64**, 108-114.
- [16] S. Zhang, Y.S. Park, J. Li, *et al.*, 2009. Negative Refractive Index in Chiral Metamaterials. *Phys. Rev. Lett.* **102**, 023901.
- [17] B. Wang, T. Koschny, and C.M. Soukoulis, 2009. Wide-angle and polarization-independent chiral metamaterial absorber. *Phys. Rev.*, B **80**, 033108.
- [18] H.T. Chen, 2012. Interference theory of metamaterial perfect absorber. *Opt. Express*, **20**, 7165-7172.
- [19] N.V. Dung, P.V. Tuong, Y.J. Yoo, *et al.*, 2015. Perfect and broad absorption by the active control of electric resonance in metamaterial. *J. Opt.*, **17**, 045105
- [20] D. R. Smith, D. C. Vier, T. Koschny, and C. M. Soukoulis, 2005. Electromagnetic parameter retrieval from inhomogeneous metamaterials. *Phys. Rev.*, E **71**, 036617.
- [21] H. Luo, Y.Z. Cheng, and R.Z. Gong, 2011. Numerical study of metamaterial absorber and extending absorbance bandwidth based on multi-square patches. *Eur. Phys. J. B*, **81**, 387-392.
- [22] N. Pouyanfar, J. Nourinia, and C. Ghobadi, 2021. Multiband and multifunctional polarization converter using an asymmetric metasurface. *Sci. Rep.*, **11**, 9306.